UNIVERSITY OF BIRMINGHAM
University of Birmingham Research at Birmingham

Native Ambient Mass Spectrometry Imaging of Ligand-Bound and Metal-Bound Proteins in Rat Brain

Sisley, Emma K; Hale, Oliver J; Styles, Iain B; Cooper, Helen J

DOI:
10.1021/jacs.1c10032

License:
Creative Commons: Attribution (CC BY)

Document Version
Publisher's PDF, also known as Version of record

Citation for published version (Harvard):
Sisley, EK, Hale, OJ, Styles, IB & Cooper, HJ 2022, 'Native Ambient Mass Spectrometry Imaging of Ligand-Bound and Metal-Bound Proteins in Rat Brain', *Journal of the American Chemical Society*, vol. 144, no. 5, pp. 2120-2128. https://doi.org/10.1021/jacs.1c10032

Link to publication on Research at Birmingham portal

General rights
Unless a licence is specified above, all rights (including copyright and moral rights) in this document are retained by the authors and/or the copyright holders. The express permission of the copyright holder must be obtained for any use of this material other than for purposes permitted by law.

•Users may freely distribute the URL that is used to identify this publication.
•Users may download and/or print one copy of the publication from the University of Birmingham research portal for the purpose of private study or non-commercial research.
•User may use extracts from the document in line with the concept of 'fair dealing' under the Copyright, Designs and Patents Act 1988 (?)
•Users may not further distribute the material nor use it for the purposes of commercial gain.

Where a licence is displayed above, please note the terms and conditions of the licence govern your use of this document.

When citing, please reference the published version.

Take down policy
While the University of Birmingham exercises care and attention in making items available there are rare occasions when an item has been uploaded in error or has been deemed to be commercially or otherwise sensitive.

If you believe that this is the case for this document, please contact UBIRA@lists.bham.ac.uk providing details and we will remove access to the work immediately and investigate.

Download date: 27. Apr. 2024

JACS
JOURNAL OF THE AMERICAN CHEMICAL SOCIETY
pubs.acs.org/JACS
Article

Native Ambient Mass Spectrometry Imaging of Ligand-Bound and Metal-Bound Proteins in Rat Brain

Emma K. Sisley, Oliver J. Hale, Iain B. Styles, and Helen J. Cooper*

Cite This: J. Am. Chem. Soc. 2022, 144, 2120−2128
Read Online

ACCESS | Metrics & More | Article Recommendations | Supporting Information

ABSTRACT: Label-free spatial mapping of the noncovalent interactions of proteins in their tissue environment has the potential to revolutionize life sciences research by providing opportunities for the interrogation of disease progression, drug interactions, and structural and molecular biology more broadly. Here, we demonstrate mass spectrometry imaging of endogenous intact noncovalent protein−ligand complexes in rat brain. The spatial distributions of a range of ligand-bound and metal-bound proteins were mapped in thin tissue sections by use of nanospray-desorption electrospray ionization. Proteins were identified directly from the tissue by top-down mass spectrometry. Three GDP-binding proteins (ADP ribosylation factor ARF3, ARF1, and GTPase Ran) were detected, identified, and imaged in their ligand-bound form. The nature of the ligand was confirmed by multiple rounds of tandem mass spectrometry. In addition, the metal-binding proteins parvalbumin-α and carbonic anhydrase 2 were detected, identified, and imaged in their native form, i.e., parvalbumin-α + $2Ca^{2+}$ and carbonic anhydrase + Zn^{2+}. GTPase Ran was detected with both GDP and Mg^{2+} bound. Several natively monomeric proteins displaying distinct spatial distributions were also identified by top-down mass spectrometry. Protein mass spectrometry imaging was achieved at a spatial resolution of 200 μm.

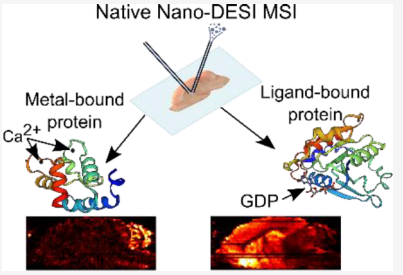

Downloaded via 2.28.186.134 on February 21, 2022 at 10:38:00 (UTC).
See https://pubs.acs.org/sharingguidelines for options on how to legitimately share published articles.

INTRODUCTION

Native ambient mass spectrometry imaging seeks to combine the benefits of native mass spectrometry and ambient mass spectrometry to visualize the spatial distribution of, and obtain structural information on, proteins and their interacting partners. In earlier work, we demonstrated native mass spectrometry imaging of folded proteins in thin sections of tissue using the ambient mass spectrometry techniques of both liquid extraction surface analysis (LESA)[1,2] and nanospray desorption electrospray ionization (nano-DESI).[3,4] The present work is the first demonstration of imaging and identification of endogenous protein−ligand and protein−metal (and protein−ligand−metal) complexes directly from tissue. These intact noncovalent complexes were spatially mapped by use of nano-DESI. The work highlights the broad specificity of ambient mass spectrometry—imaging was performed without *a priori* knowledge of the nature of the proteins or the ligands. All were identified by top-down mass spectrometry of the intact species extracted directly from the tissue.

Native mass spectrometry has become well-established as a tool for structural biology.[5] The chief benefits of native mass spectrometry derive from its ability to glean structural information in the form of stoichiometry,[6,7] stability,[8,9] and topology[10] of protein complexes. Typically, protein samples are introduced to the mass spectrometer by electrospray ionization (ESI) from a solution tailored to mimic native conditions. Noncovalent interactions present in solution phase are retained in the gas phase.

Ambient mass spectrometry refers to the direct sampling and ionization of analytes from a complex substrate, such as a tissue section, under ambient conditions and with minimal or no sample-pretreatment. These fundamental aspects of ambient mass spectrometry promote the preservation of biological information and provide opportunities for spatial mapping of analytes. Much of the published work on ambient mass spectrometry focuses on small molecules as these are easily extracted and ionized; however, since ambient mass spectrometry makes use of electrospray ionization it also lends itself to the analysis of proteins. Ambient mass spectrometry analysis of proteins to date has largely either made use of denaturing solvents[11−17] (resulting in protein unfolding) or has incorporated proteolytic digestion.[18−21]

Two ambient mass spectrometry techniques have so far been applied to native mass spectrometry imaging: LESA[1,2,22] and nano-DESI.[3,4] Both techniques involve liquid microjunction sampling of the tissue substrate; LESA[23] makes use of discrete (μL) volumes of sampling solvent, whereas nano-DESI[24] makes use of a continuous flow of sampling solvent. The sampling area associated with LESA is greater than that for nano-DESI, meaning that while LESA typically provides

Received: September 22, 2021
Published: January 25, 2022

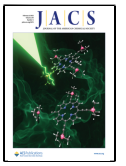

© 2022 The Authors. Published by American Chemical Society

greater sensitivity, a greater spatial resolution can be achieved by nano-DESI. The minimum pixel size afforded by LESA is 1 mm × 1 mm; however, native nano-DESI mass spectrometry imaging has been demonstrated with pixel sizes of 200 μm × 200 μm. (Nano-DESI has been demonstrated with pixel sizes of 4 μm × 10 μm for small molecules[25]).

A more general benefit of the use of (any) mass spectrometry for imaging is its broad specificity—there is no requirement for labeling or prior knowledge of the analytes. Nevertheless, once an analyte of interest has been established, e.g., through examination of single ion images or multivariate analysis of the imaging data set, it is necessary to confirm the chemical identity of that analyte. To that end, a third branch of mass spectrometry has been exploited in this work, that of top-down mass spectrometry.[26,27] In top-down mass spectrometry, intact protein ions are fragmented in the mass spectrometer (a process known as tandem mass spectrometry). The mass-to-charge (m/z) ratios of the fragments are searched against theoretical m/z values derived from protein databases and the identity of the protein confirmed. A challenge for top-down mass spectrometry, exacerbated in native ambient mass spectrometry of tissue samples, is the low relative abundance of fragment ions, a consequence of the number of degrees of freedom in large protein ions and the low abundance of the proteins themselves. In this work, we have applied three approaches for protein identification: top-down nano-DESI of tissue, top-down LESA of tissue, and LESA extraction followed by direct infusion nanoelectrospray top-down mass spectrometry. In all cases, fragmentation was induced by higher-energy collision dissociation (HCD). For protein complexes, there is an additional layer of identification required—that of the ligand. To address this issue, multiple rounds of tandem mass spectrometry (MS^n) were performed.

EXPERIMENTAL SECTION

Materials. Brain tissue from a vehicle-dosed (0.5% HPMC and 0.1% tween 80 in water) adult male Han-Wistar rat (i.e., extraneous control tissue from a drug dosing experiment) was the kind gift of Dr. Richard Goodwin (Astra Zeneca). The animal was euthanized 6 h post-dose. Dissection was performed by trained AstraZeneca staff (project license PP77366793, procedure number 3). Brains were snap-frozen in isopentane over dry ice. All tissue was stored at −80 °C before sectioning at −22 °C to a thickness of 10 μm with a CM1810 Cryostat (Leica Microsystems, Wetzlar, Germany) and thaw mounting onto glass microscope slides. Sections were stored at −80 °C until use. Tissue sections were not subjected to any washing protocol prior to analysis.

HPLC-grade water was purchased from Fisher Scientific (Loughborough, UK), C_8E_4 detergent was purchased from Sigma-Aldrich (Gillingham, UK), and HPLC grade ammonium acetate was purchased from J. T. Baker (Deventer, Netherlands).

LESA. The thaw mounted tissue was mounted onto a universal LESA adaptor plate and scanned into LESA Points at 600 dpi. For imaging, a grid of sampling points with 1 × 1 mm spacing was defined across the tissue section. "Contact" LESA[28] was performed using the Triversa Nanomate platform (Advion, Ithaca, NY) controlled by the Chipsoft software (v8.3.3, Advion). Five microliters of solvent (50 mM ammonium acetate + 0.125% C_8E_4) was aspirated from the solvent well into the conductive pipet tip. The pipet tip was relocated to a location on the tissue and 2 μL of solvent was dispensed. The solvent was held on the tissue for 45 s before 2.5 μL was reaspirated and the pipet moved to the nano-ESI chip. Nanoelectrospray was initiated using a potential of 1.65 kV and a backpressure of 0.15 PSI. For LESA tandem mass spectrometry experiments, sampling locations were defined in accordance with preceding imaging experiments. The LESA sampling procedure was as above.

For some tandem mass spectrometry experiments (see main text), LESA extraction was performed using the Advanced User Interface (AUI) in the Chipsoft software and the sample collected in a microtiter plate before being transferred to custom-made gold coated borosilicate nanoelectrospray emitters. For the extraction, half of a 96-well plate and the glass slide were mounted into the plate holder. Five microliters of solvent was aspirated from a well in the microtiter plate into the pipet. The pipet was relocated to the user-defined location on the tissue and brought into contact with the tissue where ten dispense/reaspirate cycles of 2 μL solvent were completed (providing ∼30 s of sampling). The sample was collected in a clean well of the microtiter plate before being transferred (4 μL) into gold coated borosilicate nanoelectrospray emitters. Borosilicate glass capillaries (I.D. 0.68 mm O.D. 1.2 mm) were pulled into tips using a micropipette puller (Sutter Instrument) and then sputter coated with gold using an agar sputter coater. The loaded nanoelectrospray emitter was placed into the nano-ESI source (Thermo Fisher Scientific, San Jose, CA). Nanoelectrospray was initiated using 900−1200 V.

Nano-DESI. Nano-DESI was performed using a home-built ion source adapted from a previous version[3] to allow fully automated 3-axis movement. An XYZ-stage (Zaber Technologies Inc., Vancouver, Canada) was mounted to the front of an Orbitrap Eclipse mass spectrometer (Thermo Fisher Scientific, San Jose, CA) with optomechanical components (Thorlabs Inc., Newton, New Jersey). Ion source interlocks were defeated for the mass spectrometer to recognize the nano-DESI source as a nano-ESI source. Solvent and sampling capillaries were flame-pulled from fused silica tubing (O.D. 275 μm, I.D. 75 μm prior to modification) and cut to a final outer diameter of approximately 100 μm. The exit of the sampling capillary was not flame-pulled but had the coating removed. The sampling capillary was positioned approximately 0.5 mm within the mass spectrometer inlet to achieve aspiration of solvent with the inlet vacuum. A 10 mL gastight syringe (Hamilton, Reno, NV) delivered solvent (200 mM aqueous ammonium acetate + 0.125% C_8E_4) at 2.0 μL/min to maintain a stable solvent bridge between the two capillaries. The high voltage power supply was connected directly to the syringe needle and a potential of 800 V was applied for optimal spray stability. Photographs of the nano-DESI source are shown in Figure S1, Supporting Information.

The XYZ-stage was connected through a USB 2.0 port to the mass spectrometer control PC and controlled by the manufacturer's software (v.2.6.7.429, Zaber Control) and custom software written in LabVIEW (2019, NI, Austin, Texas). An Arduino Uno v3 microcontroller (Arduino, Turin, Italy) with a relay was connected to another USB 2.0 port, and the relay was connected to the contact closure pins on the mass spectrometer.

For automated data acquisition, an instrument method was written in Xcalibur (v4.3, Thermo) using the settings described in the next section. A tissue section mounted to a glass slide was attached to the XYZ-stage. On initialization of XYZ-stage movement, contact closure was triggered via the relay and the mass spectrometer began acquiring data as defined in the instrument method. Each line scan in the nano-DESI ion image was acquired in an automated sequence over the course of approximately 8 h, during which the tissue was maintained at room temperature. The stage moved the tissue section under the nano-DESI probe at a rate of 25 μm/s, with a 200 μm step between each line scan.

Mass Spectrometry. Mass spectrometry data were acquired on an Orbitrap Eclipse Tribrid MS (Thermo) with the HMRn option. The instrument was operated in "Intact Protein" mode and at "Standard Pressure" (0.008 Torr in the IRM). The ion transfer tube temperature was set to 275 °C, the source induced dissociation voltage was set to 80 V and the s-lens RF was set to 120%. Mass spectra were acquired at a resolution of 7500 (at m/z 200) for imaging experiments and 120 000 (at m/z 200) for MS^2 experiments. AGC was set to 1250% (5×10^6 charges) and the maximum injection was set to 500 ms. For images, an m/z range of 2000−5000 was used. For MS^n experiments, m/z ranges were chosen depending on the experiment.

https://doi.org/10.1021/jacs.1c10032
J. Am. Chem. Soc. 2022, 144, 2120−2128

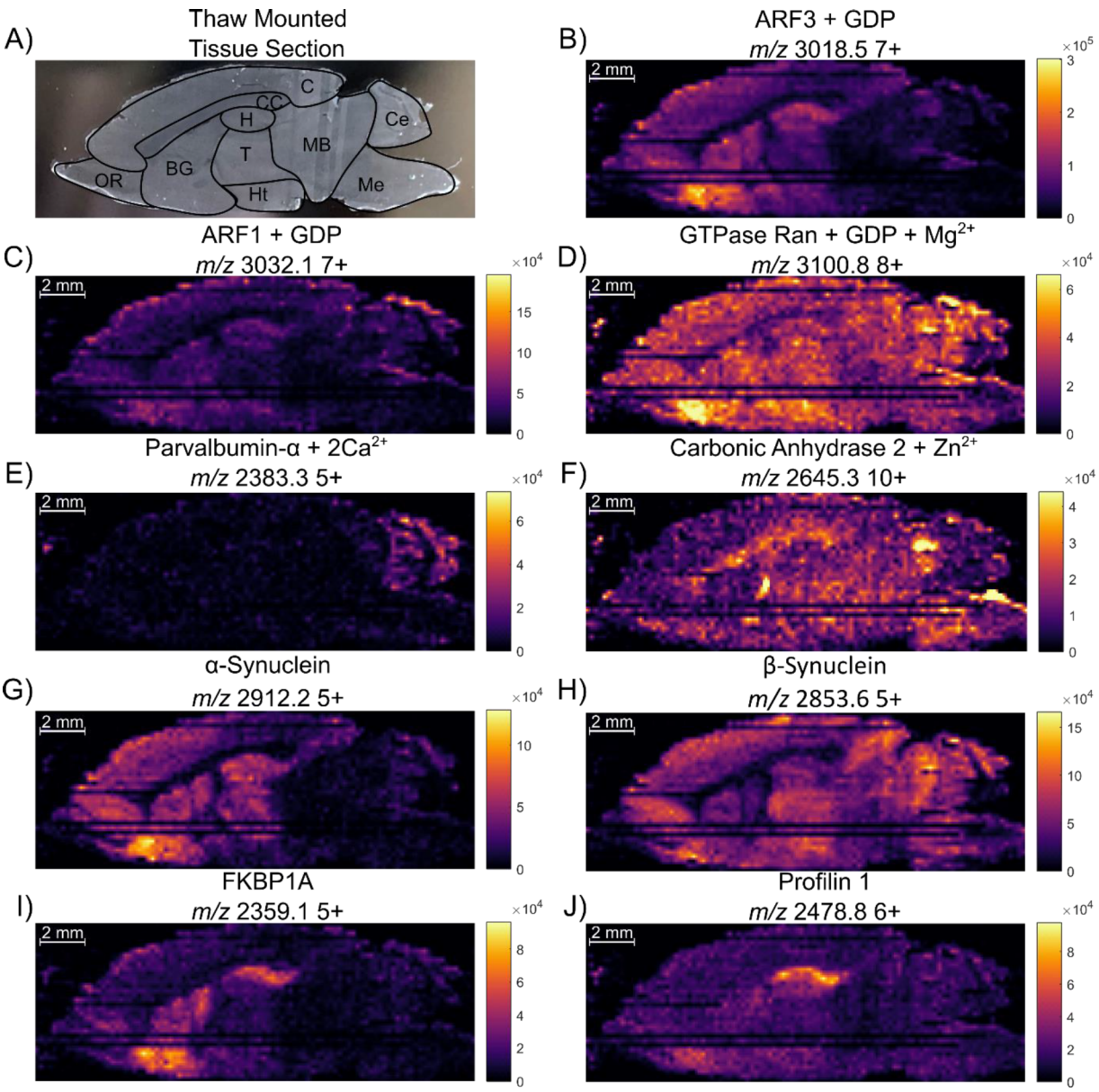

Figure 1. Native nano-DESI mass spectrometry imaging of a sagittal brain section. (A) photograph of the rat brain section before nano-DESI sampling with different regions of the brain highlighted. C, cerebral cortex; CC, corpus callosum; H, hippocampus; OR, olfactory region; BG, basal ganglia; T, thalamus; MB, mid brain; Ce, cerebellum; Ht, hypothalamus; and Me, medulla. Ion images showing the distribution of intact proteins: (B) ADP ribosylation factor 3 (ARF 3) with GDP bound, (C) ADP ribosylation factor 1 (ARF1) with GDP bound, (D) GTP-binding nuclear protein Ran (GTPase Ran) with GDP and Mg^{2+} bound, (E) Parvalbumin-α with $2Ca^{2+}$ bound, (F) Carbonic anhydrase 2 with Zn^{2+} bound, (G) α-synuclein, (H) β-synuclein, (I) peptidyl-prolyl cis−trans isomerase FKBP1A, and (J) Profilin 1. No normalization was applied to the ion images. Scale bars represent signal intensity.

For all positive mode MS^2 experiments, precursor ions were isolated in the ion trap with an isolation width of 6 m/z and a normalized collision energy (NCE) between 20 and 40% was applied (depending on the protein). All data were recorded in the Orbitrap mass analyzer. For MS^2 data acquired using nano-DESI sampling, the raster rate of the nano-DESI probe was reduced to 5 μm/s to help maintain signal intensity.[3] Table S1, Supporting Information, shows the HCD energy and sampling method used for each protein.

In some cases (see main text), nano-DESI MS^n experiments were performed in negative mode. In these experiments, the raster rate of the nano-DESI probe was 10 μm/s. Precursor ions (MS^2) were isolated in the ion trap with an isolation width of 6 m/z and fragmented by HCD using an NCE of between 20 and 30%. High m/z (1000−4000) and low m/z (200−500) data were collected in the Orbitrap mass analyzer. (It was necessary to collect high and low m/z data separately because the upper m/z in the Orbitrap mass analyzer is capped at m/z 2000 when the lower m/z is below 500). For MS^3 experiments, the precursor ions were isolated in the ion trap with isolation width 10−15 m/z and fragmented by HCD with an NCE of 25−26%. MS^3 data were recorded in the ion trap analyzer. Table S2, Supporting Information, shows the HCD parameters used for each protein.

Data Analysis. *MS Image Processing.* LESA images were produced by collecting 2 min of data per pixel. Each mass spectrum (pixel) was averaged in Freestyle (v1.4, Thermo Fisher Scientific) and exported in the Thermo .raw format. The .raw files were converted to mzML files using MSConvert (v3, Proteowizard),[29] before being converted into a single imzML file using the imzML convertor.[30] Images were produced using SpectralAnalysis.[31] Top-hat baseline subtraction (using a window of 15) was applied to the spectra. TIC

https://doi.org/10.1021/jacs.1c10032
J. Am. Chem. Soc. 2022, 144, 2120−2128

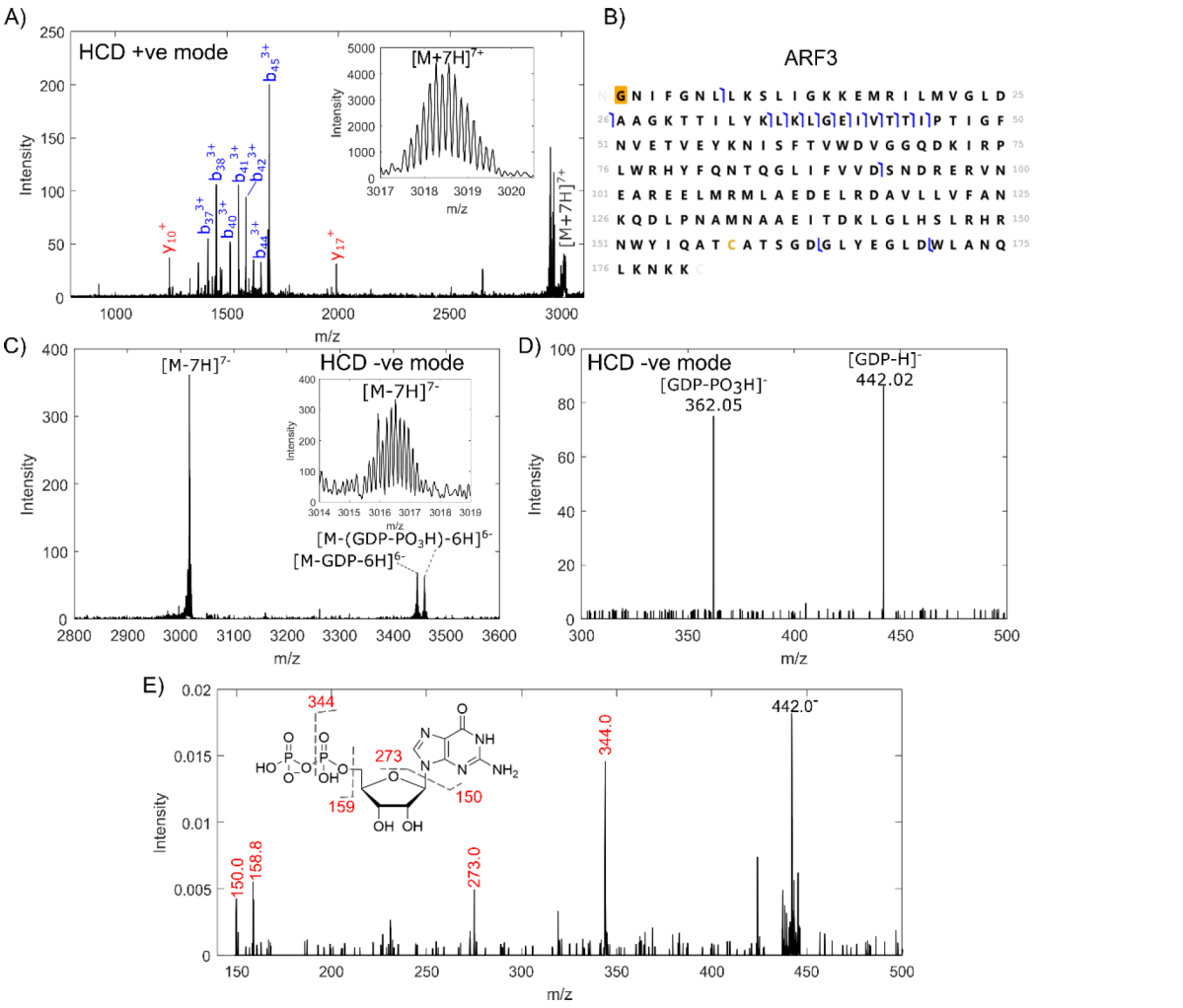

Figure 2. Identification of myristoylated ARF3 in complex with GDP. (A) Positive mode LESA HCD MS^2 (NCE 34%) of m/z 3018.2 ± 3, inset shows isolated 7+ precursor ion signal. (B) Sequence of ARF3 with observed fragments. Orange square denotes N-terminal myristoylation. (C) Negative mode nano-DESI HCD MS^2 (NCE 22%) of 3016.5 ± 3, inset showing isolated 7- precursor ion signal. (D) Low m/z ions observed from negative mode nano-DESI HCD MS^2 (NCE 22%) of 3016.5 ± 3. (E) MS^3 of $[GDP-H]^-$ (m/z 442.0 ± 5, NCE 26%), inset showing the structure of GDP and the cleavages observed.

normalization was performed to correct for variations in performance of the separate nozzles on the LESA chip.

Nano-DESI images were produced by acquiring line scans in sequence. The line scans were converted from Thermo .raw files into a single imzML file using Firefly (v3.2.0.23, Prosolia, Inc.) which summed the spectra into 8 s time bins to create 200 μm pixels. Ion images were created using MSI reader[32] with a pixel size of 200 × 200 μm^2 and linear interpolation. Ion images were created using a 0.2 m/z window across the protein signal apex. No TIC normalization was applied.

Intact Mass Analysis. Protein monoisotopic masses were determined using the Xtract algorithm in the Freestyle software (v1.4, Thermo Fisher Scientific).

Protein Identifications. Proteins from MS^2 spectra were identified using ProSight 4.1 (Thermo Fisher Scientific). Searches were performed against the *Rattus norvegicus* proteome (downloaded from Proteinacious.net July 2020). Precursor mass tolerance was set to 1 kDa to allow for hits including small bound ligands, the fragment ion tolerance was set to 30 ppm and a minimum fragment match of 2. Protein assignments were manually confirmed using Protein Prospector (v6.3.1, https://prospector.ucsf.edu/prospector/mshome.htm, UCSF).

RESULTS AND DISCUSSION

Figure 1 shows a photograph of the sagittal brain section and native nano-DESI ion images of a range of proteins. Corresponding LESA images of adjacent sections are shown in Figure S2, Supporting Information. There is generally good agreement between the nano-DESI and LESA images despite the lower spatial resolution of LESA, although some features appear widened in the LESA images due to the larger sampling area. The horizontal black lines seen in the bottom half of the nano-DESI images correspond to "dead" pixels in which the nano-DESI probe has blocked. Their presence illustrates the delicate nature of the technique. The proteins ADP ribosylation factor (ARF) 3, ARF1, and GTPase Ran were detected in their native ligand-bound form, i.e., with guanosine diphosphate, GDP, noncovalently attached to the polypeptide. The proteins GTPase Ran, parvalbumin-α, and carbonic anhydrase were detected in their metal-bound forms. The proteins α-synuclein, β-synuclein, peptidyl-prolyl cis−trans isomerase FKBP1A (FKBP1A), and profilin 1 are free monomers in their native state and each display distinctive spatial distributions. Figure S3, Supporting Information, shows additional nano-DESI images of monomeric proteins phos-

https://doi.org/10.1021/jacs.1c10032
J. Am. Chem. Soc. 2022, 144, 2120−2128

phatidylethanolamine-binding protein 1 (PEBP1), peptidyl-prolyl cis−trans isomerase A (PPIA), and coactosin-like protein. With the exception of PEBP1, which was observed following native nano-DESI of rat kidney,[3] none of these proteins have previously been detected by native ambient mass spectrometry, and were identified here by top-down fragmentation as described below. Figure S4, Supporting Information, shows summed mass spectra from different regions of the brain (cortex, cerebellum, and hippocampus).

Figure 1B shows the spatial distribution of 7+ ions (m/z 3018.5) of ADP ribosylation factor 3 (ARF3), revealing its presence in the cerebral cortex, hippocampus, basal ganglia, olfactory region, thalamus, and hypothalamus, in agreement with previous gene expression experiments.[33] The exact nature of the protein was confirmed via a series of tandem mass spectrometry experiments. First, the cerebral cortex region of an adjacent tissue section was sampled with LESA and the 7+ ions were subjected to higher-energy collision dissociation (HCD), see Figure 2A and 2B. The observed backbone fragments confirmed the protein identity as ARF3. The results also revealed that the protein is myristoylated at the N-terminus. Myristoylation is the covalent attachment of a 14-carbon fatty acid on an N-terminal glycine, resulting in a 210 Da mass shift, and is commonly involved in protein interactions with lipid membranes.[34]

The ARFs are a family of GTP-binding proteins which regulate membrane traffic and structure.[35] ARF3 cycles between a (nonactive) cytosolic GDP-bound form and an (active) membrane-associated GTP-bound form. This switch causes a conformational change in the protein. In the GDP-bound form, the myristoylated N-terminus is tucked within the protein while in the GTP bound form the myristoylation is exposed enabling interaction with membranes.[36] The mono-isotopic mass of GDP is 443.0 Da, which corresponds to the difference between the measured mass of the protein (21109.7 Da) and the calculated mass based on the primary sequence with myristoylation (20666.8 Da). The HCD mass spectrum (Figure 2A) does not, however, reveal peaks corresponding to loss of a ligand of mass 443 Da; rather, a series of peaks corresponding to neutral losses of 362 and 460 Da from the precursor ions are observed. These neutral losses are also observed when the HCD collision energy is lowered below the threshold for backbone fragmentation along with an additional peak corresponding to a loss of 282 Da (Figure S5, Supporting Information).

To confirm the presence of bound GDP, we performed multiple-stage tandem mass spectrometry (MS^3) by use of native nano-DESI in negative ion mode. Figure S6, Supporting Information, shows the mass spectrum obtained from a nano-DESI line scan in the lower basal ganglia region of an adjacent section. The 7− ions at m/z 3016.5 were isolated and fragmented by HCD, see Figure 2C and 2D. In the higher m/z range, the dominant fragments were 6− ions corresponding to losses of 362 and 442 Da from the precursor. In the lower m/z range, singly charged peaks at m/z 442 and 362 corresponding to $[GDP\text{-}H]^-$ and $[GDP\text{-}PO_3H]^-$ were observed. The ions with m/z 442 were isolated and further fragmented by HCD (Figure 2E). The results confirm the identity of the ligand as GDP and are in good agreement with tandem mass spectra of the free mononucleotide.[37] On the basis of this information, the positive mode HCD spectra were revisited and fragmentation pathways proposed (Figure S5, Supporting Information). The structure of the ARF3-GDP complex is shown in Figure S7, Supporting Information, revealing hydrogen bonds between the GDP and threonine and aspartic acid OH groups. We hypothesize that the 460 Da loss corresponds to loss of GDP combined with amino acid side-chain cleavage (loss of an OH group). Interestingly, the fragmentation pathway of the GDP molecule seems to differ depending on whether fragmentation occurs when the GDP is bound to the protein (MS^2; loss of a phosphoryl group) or in the free GDP anion (MS^3; loss of a phosphate group).

ADP ribosylation factor 1 (ARF1) (Figure 1C) is also a member of the ARF family and cycles between a GDP- and GTP-bound form. Its spatial distribution is similar to that of ARF3 but the signal is approximately 1 order of magnitude lower. ARF1 was identified following LESA sampling of an adjacent section followed by HCD of the 7+ precursor ions (Figure S8, Supporting Information). The observed backbone fragments confirm both the protein identity and N-terminal myristoylation. The remaining 443 Da mass shift corresponds to GDP, whose presence is further confirmed by the fragment at m/z 2980.4 which derives from the cleavage of the ligand's phosphoryl group. The measured mass of the protein (21206.6 Da) is in good agreement with the calculated mass of the myristoylated ARF1 with bound GDP (21026.0 Da).

Figure 1D shows the spatial distribution of GTP-binding nuclear protein Ran (GTPase Ran). The protein is observed throughout the brain, with a lower abundance in the corpus callosum, mid brain and medulla. GTPase Ran switches between a GTP- and GDP-bound form, in which the GDP-bound form is typically cytosolic while the GTP-bound form is nuclear.[38] GTPase Ran is required for protein import into the nucleus during interphase as well as being involved in spindle assembly during mitosis.[39] It has also been noted that its expression is reduced in Alzheimer's disease.[40] In these experiments, the protein was observed in complex with GDP and a magnesium cation as confirmed by a series of tandem mass spectrometry measurements. HCD fragmentation of the 9+ ions observed following nano-DESI did not result in any backbone fragments; however, two peaks corresponding to neutral losses of 362 and 460 Da from the precursor ions were observed (Figure S9A, Supporting Information). This fragmentation pattern is similar to that seen in positive mode for the GDP-bound ARF proteins described above. It is likely the GDP ligand is more sensitive to fragmentation compared to the protein due to the phosphate groups in the ligand, which are known to cleave preferentially in collision induced fragmentation.[41] An adjacent tissue section was subjected to LESA extraction and the resulting sample collected before being introduced to the mass spectrometer by nanoelectrospray ionization using custom-made gold-coated borosilicate tips. The 9+ protein precursor ions were selected and subjected to HCD. A single backbone fragment adjacent to aspartic acid D17 was observed (Figure S9B and S9C, Supporting Information). Preferential cleavage at aspartic acid residues is a well-known feature of native collision-induced top-down mass spectrometry.[27,42] To confirm the presence of bound GDP, we performed multiple-stage tandem mass spectrometry (MS^3) by use of native nano-DESI in negative mode. The 8− ions at m/z 3098.5 were selected and subjected to HCD (Figure S10, Supporting Information). In the high m/z range, the dominant fragments were 7− ions corresponding to losses of 362 and 442 Da. In the low m/z range, peaks at m/z 442 and 362 corresponding to $[GDP\text{-}H]^-$ and $[GDP\text{-}PO3H]^-$ were observed. The fragment ions at m/z

https://doi.org/10.1021/jacs.1c10032
J. Am. Chem. Soc. 2022, 144, 2120−2128

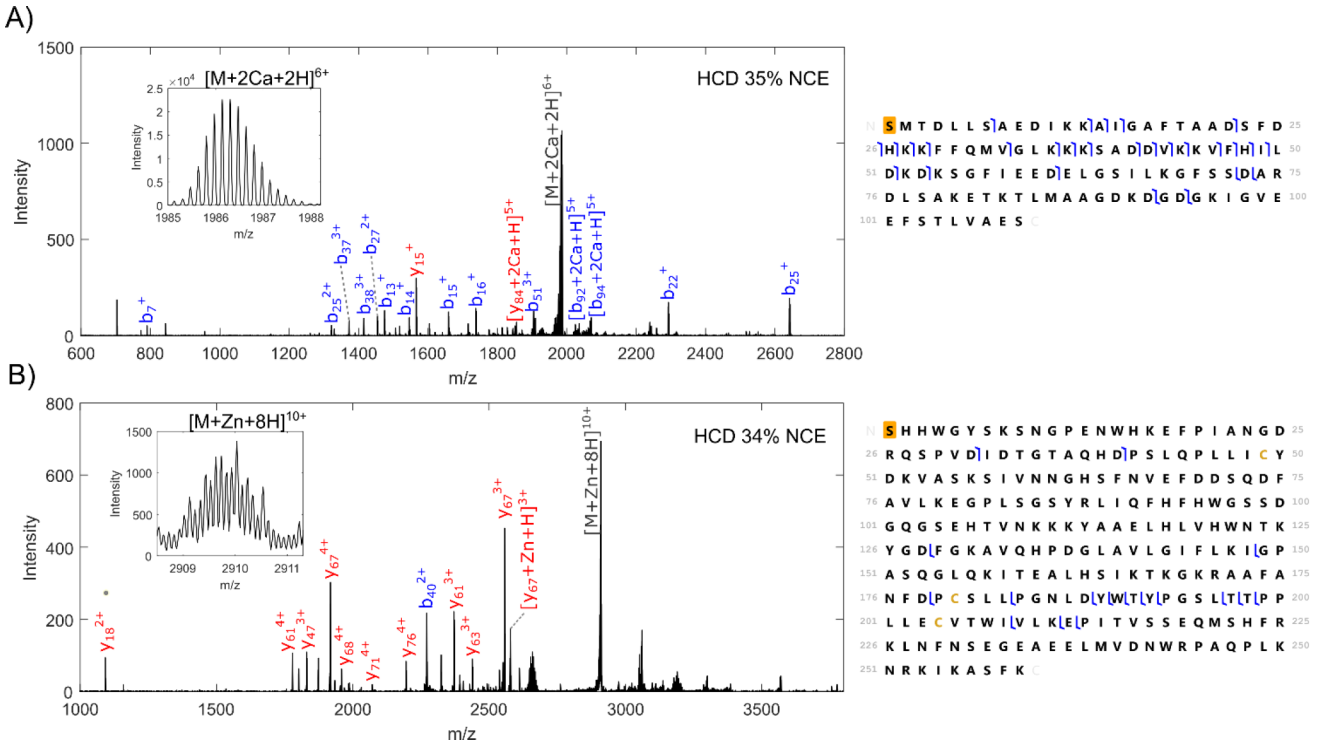

Figure 3. Identification of protein-metal complexes. (A) (Left) HCD MS^2 of 6+ ions of N-terminally acetylated parvalbumin-α with $2Ca^{2+}$ ions bound (m/z 1986.2 ± 3, NCE 35%), inset shows isolated 6+ precursor. (Right) Protein sequence with cleavages observed. (B) (Left) HCD MS^2 of 10+ ions of N-terminally acetylated carbonic anhydrase 2 with Zn^{2+} ion bound (m/z 2909.7 ± 3, NCE 34%), inset shows isolated 10+ precursor ion signal. (Right) Protein sequence with cleavages observed.

442 were selected for a further round of HCD which confirmed the identity of the ligand as GDP. The remaining mass shift between the measured mass of the protein (24783.5 Da) and the mass calculated on the basis of the primary sequence plus GDP (24761.7 Da) is 22 Da, corresponding to the presence of the Mg^{2+} cofactor.[43]

Other metal-bound proteins were detected in the native nano-DESI analysis of the brain. Figure 1E shows the distribution of calcium-bound parvalbumin-α, revealing its presence in the cerebellum, in agreement with the literature where it has been shown to be particularly enriched in specific cerebral neurons.[44] Parvalbumin-α is a calcium binding protein and has 3 EF hand (helix−loop−helix) motifs of which only 2 bind Ca^{2+}. The measured mass (11904.7 Da) corresponds to the mass of the N-terminal acetylated polypeptide plus two calcium ions (calculated mass 11905.1 Da). The protein was identified by tandem mass spectrometry experiments in which an adjacent section was microextracted by LESA and the resulting sample introduced to the mass spectrometer via nanoelectrospray with custom-made gold-coated borosilicate tips. The 6+ ions (m/z 1986.2) were selected and subjected to HCD (Figure 3A). A number of backbone fragments were observed, confirming the identity of the protein and the presence of N-terminal acetylation, some of which retained the metal ions. Parvalbumin-α has previously been detected in a top-down LC-MS analysis of mouse brain homogenates along with α-synculein, β-synuclein, FKBP1A, and PEBP1.[45]

Figure 1F shows the distribution of zinc-bound carbonic anhydrase 2 (CA2). CA2 catalyzes the interconversion of CO_2 and bicarbonate, with the zinc ion acting as the catalytic site. CA2 is found in glial cells, which make up a high percentage of the corpus callosum, explaining the observed distribution.[46]

The measured mass of the protein 29070.2 Da is in good agreement with the calculated mass (29069.9 Da) of the N-terminally acetylated holoprotein. The protein was identified following HCD of the 10+ precursor ions observed from a microextracted LESA sample which was subsequently subjected to nanoelectrospray ionization (Figure 3B). A number of backbone fragments were observed, some of which retained the Zn^{2+} ion.

In addition to the endogenous ligand-bound and metal-bound protein complexes described above, a number of monomeric proteins were identified that displayed distinctive spatial distributions. The ion image shown in Figure 1G corresponds to α-synuclein, with signal observed in the cerebral cortex, hippocampus, basal ganglia, olfactory region, thalamus, and cerebellum, is in agreement with previous biochemical measurements[47,48] as well as MSI of a C-terminal fragment of α-synuclein in regions of mouse brain.[18] The exact function of α-synuclein in healthy tissue is still not fully understood, although it is widely accepted that it is involved in cell signaling. α-Synuclein is better known for its involvement in Parkinson's disease where it has been found to oligomerize and become the main component of Lewy bodies. The identity of the protein was confirmed by LESA tandem mass spectrometry (see Figure S11, Supporting Information), which also revealed it to be N-terminally acetylated (measured mass 14548.0 Da, calculated mass 14548.2). α-Synuclein is part of a family of synucleins (α, β, and γ) and the presence of truncated β-synuclein was also confirmed by tandem mass spectrometry (see Figure S12, Supporting Information). The results show the protein to be N-terminally acetylated and truncated at the C-terminus through loss of the three C-terminal amino acid residues (KGP) (measured mass 14254.8

https://doi.org/10.1021/jacs.1c10032
J. Am. Chem. Soc. 2022, 144, 2120−2128

Da, calculated mass 14254.9 Da). β-Synuclein has been reported to be an inhibitor of α-synuclein aggregation in Parkinson's disease.[49,50] The distribution of β-synuclein (Figure 1H) is noticeably different to that of α-synuclein, with signal observed throughout the brain but absent in the corpus callosum.

Peptidyl-prolyl cis−trans isomerase FKBP1A (FKBP1A, also known as FKBP12) and profilin 1 were also observed to have very specific distributions in the brain. Figure 1I shows FKBPA1 is expressed in the hippocampus and basal ganglia. There is also a weaker signal for the protein in the cerebral cortex. FKBPA1 (measured mass 17731.5 Da, calculated mass 17731.7 Da) was identified by tandem mass spectrometry using nano-DESI (Figure S13, Supporting Information).[45] Figure 1J shows profilin-1 (measured mass 14858.3 Da, calculated mass 14858.4 Da) to have a higher expression in the hippocampus compared with the rest of the tissue. The protein was identified by tandem mass spectrometry following LESA microextraction of an adjacent tissue section (Figure S14, Supporting Information). Profilin 1 is expressed in most tissues and makes up about 0.05% of proteins in the brain.[51] The protein is involved in the regulation of actin polymerization.[52]

Other proteins identified from the brain include phosphatidylethanolamine-binding protein 1 (PEBP1), peptidyl-prolyl cis−trans isomerase A (PPIA) and coactosin-like protein (for images, see Figure S3, Supporting Information). PEBP1, also known as Raf kinase inhibitor protein (RKIP), is one of the most dominant signals observed in both the LESA mass spectra and the nano-DESI mass spectra. PEBP1 (measured mass 20699.1 Da, calculated mass 20699.3 Da) was identified using LESA tandem mass spectrometry (Figure S15, Supporting Information). PEBP1 has also been detected in previous nano-DESI imaging experiments of the kidney where it was also found to have a ubiquitous distribution across the tissue with the exception of blood vessel features.[3] PEBP1 is known to be involved in the regulation of cell proliferation and differentiation,[53] and is involved in some neurological diseases including Alzheimer's disease, depression and brain tumors.[54] PPIA (measured mass 17731.5 Da, calculated mass 17731.7 Da) was also detected throughout the tissue and was observed both with and without acetylation. PPIA was identified by tandem mass spectrometry experiments following LESA microextraction of an adjacent tissue section (Figure S16, Supporting Information). Coactosin-like protein (measured mass 15832.7 Da, calculated mass 15832.9 Da) was detected at higher intensity in the hippocampus and was identified by tandem mass spectrometry experiments following LESA microextraction of an adjacent tissue section (Figure S17, Supporting Information). This protein has been linked to the progression of glioblastomas.[55]

CONCLUSION

The results demonstrate the mass spectrometry imaging and identification of a range of endogenous ligand-bound and metal-bound protein complexes, in addition to some monomeric proteins with particularly distinct spatial distributions, directly from tissue sections of rat brain at 200 μm spatial resolution. For the protein−ligand complexes, the protein was identified by positive mode top-down mass spectrometry, and the ligand identified by MS^3 tandem mass spectrometry using negative mode nano-DESI. Choice of sampling approach for top-down mass spectrometry was informed by location and abundance of the protein of interest. Broadly distributed proteins are suitable for nano-DESI tandem mass spectrometry, whereas more localized proteins require LESA tandem mass spectrometry, and those of very low abundance require LESA extraction and separate infusion via gold-coated borosilicate tips which provide enhanced nanoelectrospray stability over extended periods. In total, 12 proteins were identified, none of which have been previously observed in ambient mass spectrometry imaging of brain tissue (although one has been observed in kidney tissue). Importantly, the proteins identified are presented as an example of the capabilities of native ambient mass spectrometry of brain, and do not constitute the limits of the approach.

The ability to perform untargeted label-free spatial mapping of the noncovalent interactions of proteins, while also identifying both the protein and its ligands, offers great potential for structural biology and translation to biomedicine. For example, native ambient mass spectrometry imaging could be applied to understanding diseases caused by misfolding of proteins and protein aggregation such as Alzheimer's, Huntington's, and Parkinson's disease.[56] Parkinson's disease involves the aggregation of α-synuclein, a protein identified in this study. Another potential application is the study of the mechanisms of heavy metal toxicity, which have also been linked with protein misfolding and aggregation.[57] A further application is the study of the interactions of proteins with exogenous compounds such as pharmaceuticals. The next step in all these cases is to apply native ambient mass spectrometry imaging to animal models or biopsy samples from individuals with the disease. Depending on the application, it is likely that improvements in sensitivity and/or spatial resolution will be required, and work in this area is ongoing.

ASSOCIATED CONTENT

Supporting Information

The Supporting Information is available free of charge at https://pubs.acs.org/doi/10.1021/jacs.1c10032.

Photograph of nano-DESI source (Figure S1); MS2 and MS3 HCD parameters (Tables S1 and S2); Comparison of nano-DESI and LESA ion images (Figure S2); Additional nano-DESI ion images (Figure S3); Nano-DESI mass spectra (Figure S4); HCD fragmentation of Arf3, Arf1, GTPase Ran, α-synuclein, β-synuclein, profilin 1, PEBP1, PPIA, and coactosin-like protein (Figures S5, S8−S17); negative mode nano-DESI line scan (Figure S6); structure of ARF3+GDP (Figure S7) (PDF)

AUTHOR INFORMATION

Corresponding Author

Helen J. Cooper − *School of Biosciences, University of Birmingham, Birmingham B15 2TT, U.K.*; orcid.org/0000-0003-4590-9384; Email: h.j.cooper@bham.ac.uk

Authors

Emma K. Sisley − *School of Biosciences, University of Birmingham, Birmingham B15 2TT, U.K.*

Oliver J. Hale − *School of Biosciences, University of Birmingham, Birmingham B15 2TT, U.K.*

Iain B. Styles − *School of Computer Science, University of Birmingham, Birmingham B15 2TT, U.K.; The Alan Turing Institute, London NW1 2DB, U.K.; Centre of Membrane Proteins and Receptors (COMPARE), University of*

Birmingham, Birmingham B15 2TT, U.K.; University of Nottingham, Midlands NG7 2RD, U.K.

Complete contact information is available at: https://pubs.acs.org/10.1021/jacs.1c10032

Notes

The authors declare no competing financial interest.

Supplementary data supporting this research is openly available from 10.25500/edata.bham.00000734.

■ ACKNOWLEDGMENTS

H.J.C. is an EPSRC Established Career Fellow (EP/S002979/1). E.K.S. is funded by the University of Birmingham, O.J.H. is funded by EPSRC (EP/S002979/1). The Orbitrap Eclipse mass spectrometer used in this work was funded by BBSRC (BB/S019456/1).

■ REFERENCES

(1) Griffiths, R. L.; Sisley, E. K.; Lopez-Clavijo, A. F.; Simmonds, A. L.; Styles, I. B.; Cooper, H. J. Native mass spectrometry imaging of intact proteins and protein complexes in thin tissue sections. *Int. J. Mass Spectrom.* **2019**, *437*, 23−29.

(2) Hale, O. J.; Cooper, H. J. Native Mass Spectrometry Imaging and In Situ Top-Down Identification of Intact Proteins Directly from Tissue. *J. Am. Soc. Mass Spectrom.* **2020**, *31*, 2531−2537.

(3) Hale, O. J.; Cooper, H. J. Native Mass Spectrometry Imaging of Proteins and Protein Complexes by Nano-DESI. *Anal. Chem.* **2021**, *93*, 4619−4627.

(4) Hale, O. J.; Hughes, J. W.; Cooper, H. J. Simultaneous spatial, conformational, and mass analysis of intact proteins and protein assemblies by nano-DESI travelling wave ion mobility mass spectrometry imaging. *Int. J. Mass Spectrom.* **2021**, *468*, 116656.

(5) Leney, A. C.; Heck, A. J. R. Native Mass Spectrometry: What is in the Name? *J. Am. Soc. Mass Spectrom.* **2017**, *28*, 5−13.

(6) Hernández, H.; Robinson, C. V. Determining the stoichiometry and interactions of macromolecular assemblies from mass spectrometry. *Nat. Protoc* **2007**, *2*, 715−726.

(7) Moini, M. Metal displacement and stoichiometry of protein-metal complexes under native conditions using capillary electrophoresis/mass spectrometry. *Rapid Commun. Mass Spectrom.* **2010**, *24*, 2730−2734.

(8) Niu, S.; Ruotolo, B. T. Collisional unfolding of multiprotein complexes reveals cooperative stabilization upon ligand binding. *Protein Sci.* **2015**, *24*, 1272−1281.

(9) Allison, T. M.; Reading, E.; Liko, I.; Baldwin, A. J.; Laganowsky, A.; Robinson, C. V. Quantifying the stabilizing effects of protein−ligand interactions in the gas phase. *Nat. Commun.* **2015**, *6*, 8551.

(10) Sahasrabuddhe, A.; Hsia, Y.; Busch, F.; Sheffler, W.; King, N. P.; Baker, D.; Wysocki, V. H. Confirmation of intersubunit connectivity and topology of designed protein complexes by native MS. *Proc. Natl. Acad. Sci. U. S. A.* **2018**, *115*, 1268−1273.

(11) Edwards, R. L.; Creese, A. J.; Baumert, M.; Griffiths, P.; Bunch, J.; Cooper, H. J. Hemoglobin Variant Analysis via Direct Surface Sampling of Dried Blood Spots Coupled with High-Resolution Mass Spectrometry. *Anal. Chem.* **2011**, *83*, 2265−2270.

(12) Sarsby, J.; Martin, N. J.; Lalor, P. F.; Bunch, J.; Cooper, H. J. Top-Down and Bottom-Up Identification of Proteins by Liquid Extraction Surface Analysis Mass Spectrometry of Healthy and Diseased Human Liver Tissue. *Journal of The American Society for Mass Spectrometry* **2014**, *25*, 1953−1961.

(13) Griffiths, R. L.; Creese, A. J.; Race, A. M.; Bunch, J.; Cooper, H. J. LESA FAIMS Mass Spectrometry for the Spatial Profiling of Proteins from Tissue. *Anal. Chem.* **2016**, *88*, 6758−6766.

(14) Garza, K. Y.; Feider, C. L.; Klein, D. R.; Rosenberg, J. A.; Brodbelt, J. S.; Eberlin, L. S. Desorption Electrospray Ionization Mass Spectrometry Imaging of Proteins Directly from Biological Tissue Sections. *Analytical chemistry* **2018**, *90*, 7785−7789.

(15) Towers, M. W.; Karancsi, T.; Jones, E. A.; Pringle, S. D.; Claude, E. Optimised Desorption Electrospray Ionisation Mass Spectrometry Imaging (DESI-MSI) for the Analysis of Proteins/Peptides Directly from Tissue Sections on a Travelling Wave Ion Mobility Q-ToF. *J. Am. Soc. Mass Spectrom.* **2018**, *29*, 2456−2466.

(16) Hsu, C. C.; Chou, P. T.; Zare, R. N. Imaging of Proteins in Tissue Samples Using Nanospray Desorption Electrospray Ionization Mass Spectrometry. *Anal. Chem.* **2015**, *87*, 11171−11175.

(17) Lin, L.-E.; Chen, C.-L.; Huang, Y.-C.; Chung, H.-H.; Lin, C.-W.; Chen, K.-C.; Peng, Y.-J.; Ding, S.-T.; Wang, M.-Y.; Shen, T.-L.; Hsu, C.-C. Precision biomarker discovery powered by microscopy image fusion-assisted high spatial resolution ambient ionization mass spectrometry imaging. *Anal. Chim. Acta* **2020**, *1100*, 75−87.

(18) Ryan, D. J.; Patterson, N. H.; Putnam, N. E.; Wilde, A. D.; Weiss, A.; Perry, W. J.; Cassat, J. E.; Skaar, E. P.; Caprioli, R. M.; Spraggins, J. M. MicroLESA: Integrating Autofluorescence Microscopy, In Situ Micro-Digestions, and Liquid Extraction Surface Analysis for High Spatial Resolution Targeted Proteomic Studies. *Anal. Chem.* **2019**, *91*, 7578−7585.

(19) Piehowski, P. D.; Zhu, Y.; Bramer, L. M.; Stratton, K. G.; Zhao, R.; Orton, D. J.; Moore, R. J.; Yuan, J.; Mitchell, H. D.; Gao, Y.; Webb-Robertson, B.-J. M.; Dey, S. K.; Kelly, R. T.; Burnum-Johnson, K. E. Automated mass spectrometry imaging of over 2000 proteins from tissue sections at 100-μm spatial resolution. *Nat. Commun.* **2020**, *11*, 8.

(20) Wisztorski, M.; Quanico, J.; Franck, J.; Fatou, B.; Salzet, M.; Fournier, I. Droplet-Based Liquid Extraction for Spatially-Resolved Microproteomics Analysis of Tissue Sections. *Methods Mol. Biol.* **2017**, *1618*, 49−63.

(21) Quanico, J.; Franck, J.; Cardon, T.; Leblanc, E.; Wisztorski, M.; Salzet, M.; Fournier, I. NanoLC-MS coupling of liquid microjunction microextraction for on-tissue proteomic analysis. *Biochimica et Biophysica Acta (BBA) - Proteins and Proteomics* **2017**, *1865*, 891−900.

(22) Hale, O. J.; Sisley, E. K.; Griffiths, R. L.; Styles, I. B.; Cooper, H. J. Native LESA TWIMS-MSI: Spatial, Conformational, and Mass Analysis of Proteins and Protein Complexes. *J. Am. Soc. Mass Spectrom.* **2020**, *31*, 873−879.

(23) Kertesz, V.; Van Berkel, G. J. Fully automated liquid extraction-based surface sampling and ionization using a chip-based robotic nanoelectrospray platform. *Journal of Mass Spectrometry* **2010**, *45*, 252−260.

(24) Roach, P. J.; Laskin, J.; Laskin, A. Nanospray desorption electrospray ionization: an ambient method for liquid-extraction surface sampling in mass spectrometry. *Analyst* **2010**, *135*, 2233−2236.

(25) Nguyen, S. N.; Sontag, R. L.; Carson, J. P.; Corley, R. A.; Ansong, C.; Laskin, J. Towards High-Resolution Tissue Imaging Using Nanospray Desorption Electrospray Ionization Mass Spectrometry Coupled to Shear Force Microscopy. *J. Am. Soc. Mass Spectrom.* **2018**, *29*, 316−322.

(26) Toby, T. K.; Fornelli, L.; Kelleher, N. L. Progress in Top-Down Proteomics and the Analysis of Proteoforms. *Annu. Rev. Anal Chem. (Palo Alto Calif)* **2016**, *9*, 499−519.

(27) Ives, A. N.; Su, T.; Durbin, K. R.; Early, B. P.; dos Santos Seckler, H.; Fellers, R. T.; LeDuc, R. D.; Schachner, L. F.; Patrie, S. M.; Kelleher, N. L. Using 10,000 Fragment Ions to Inform Scoring in Native Top-down Proteomics. *J. Am. Soc. Mass Spectrom.* **2020**, *31*, 1398−1409.

(28) Randall, E. C.; Bunch, J.; Cooper, H. J. Direct Analysis of Intact Proteins from Escherichia coli Colonies by Liquid Extraction Surface Analysis Mass Spectrometry. *Anal. Chem.* **2014**, *86*, 10504−10510.

(29) Chambers, M. C.; Maclean, B.; Burke, R.; Amodei, D.; Ruderman, D. L.; Neumann, S.; Gatto, L.; Fischer, B.; Pratt, B.; Egertson, J.; Hoff, K.; Kessner, D.; Tasman, N.; Shulman, N.; Frewen, B.; Baker, T. A.; Brusniak, M.-Y.; Paulse, C.; Creasy, D.; Flashner, L.; et al. A cross-platform toolkit for mass spectrometry and proteomics. *Nat. Biotechnol.* **2012**, *30*, 918−920.

(30) Race, A. M.; Styles, I. B.; Bunch, J. Inclusive sharing of mass spectrometry imaging data requires a converter for all. *Journal of Proteomics* **2012**, *75*, 5111−5112.
(31) Race, A. M.; Palmer, A. D.; Dexter, A.; Steven, R. T.; Styles, I. B.; Bunch, J. SpectralAnalysis: Software for the Masses. *Anal. Chem.* **2016**, *88*, 9451−9458.
(32) Robichaud, G.; Garrard, K. P.; Barry, J. A.; Muddiman, D. C. MSiReader: An Open-Source Interface to View and Analyze High Resolving Power MS Imaging Files on Matlab Platform. *J. Am. Soc. Mass Spectrom.* **2013**, *24*, 718−721.
(33) Suzuki, I.; Owada, Y.; Suzuki, R.; Yoshimoto, T.; Kondo, H. Localization of mRNAs for six ARFs (ADP-ribosylation factors) in the brain of developing and adult rats and changes in the expression in the hypoglossal nucleus after its axotomy. *Mol. Brain Res.* **2001**, *88*, 124−134.
(34) Udenwobele, D. I.; Su, R.-C.; Good, S. V.; Ball, T. B.; Varma Shrivastav, S.; Shrivastav, A. Myristoylation: An Important Protein Modification in the Immune Response. *Front. Immunol.* **2017**, *8*, 751.
(35) Donaldson, J. G. Filling in the GAPs in the ADP-ribosylation factor story. *Proc. Natl. Acad. Sci. U. S. A.* **2000**, *97*, 3792−3794.
(36) Liu, Y.; Kahn, R. A.; Prestegard, J. H. Structure and membrane interaction of myristoylated ARF1. *Structure* **2009**, *17*, 79−87.
(37) Strzelecka, D.; Chmielinski, S.; Bednarek, S.; Jemielity, J.; Kowalska, J. Analysis of mononucleotides by tandem mass spectrometry: investigation of fragmentation pathways for phosphate- and ribose-modified nucleotide analogues. *Sci. Rep.* **2017**, *7*, 8931.
(38) Boudhraa, Z.; Carmona, E.; Provencher, D.; Mes-Masson, A.-M. Ran GTPase: A Key Player in Tumor Progression and Metastasis. *Front. Cell Dev. Biol.* **2020**, *8*, 345.
(39) Abu-Arish, A.; Kalab, P.; Ng-Kamstra, J.; Weis, K.; Fradin, C. Spatial distribution and mobility of the Ran GTPase in live interphase cells. *Biophys. J.* **2009**, *97*, 2164−2178.
(40) Mastroeni, D.; Chouliaras, L.; Grover, A.; Liang, W. S.; Hauns, K.; Rogers, J.; Coleman, P. D. Reduced RAN expression and disrupted transport between cytoplasm and nucleus; a key event in Alzheimer's disease pathophysiology. *PLoS One* **2013**, *8*, e53349−e53349.
(41) Potel, C. M.; Lemeer, S.; Heck, A. J. R. Phosphopeptide Fragmentation and Site Localization by Mass Spectrometry: An Update. *Anal. Chem.* **2019**, *91*, 126−141.
(42) Haverland, N. A.; Skinner, O. S.; Fellers, R. T.; Tariq, A. A.; Early, B. P.; LeDuc, R. D.; Fornelli, L.; Compton, P. D.; Kelleher, N. L. Defining Gas-Phase Fragmentation Propensities of Intact Proteins During Native Top-Down Mass Spectrometry. *Journal of The American Society for Mass Spectrometry* **2017**, *28*, 1203−1215.
(43) Rudack, T.; Jenrich, S.; Brucker, S.; Vetter, I. R.; Gerwert, K.; Kötting, C. Catalysis of GTP Hydrolysis by Small GTPases at Atomic Detail by Integration of X-ray Crystallography, Experimental, and Theoretical IR Spectroscopy*. *J. Biol. Chem.* **2015**, *290*, 24079−24090.
(44) Schwaller, B.; Meyer, M.; Schiffmann, S. 'New' functions for 'old' proteins: The role of the calcium-binding proteins calbindin D-28k, calretinin and parvalbumin, in cerebellar physiology. Studies with knockout mice. *Cerebellum* **2002**, *1*, 241−258.
(45) Davis, R. G.; Park, H.-M.; Kim, K.; Greer, J. B.; Fellers, R. T.; LeDuc, R. D.; Romanova, E. V.; Rubakhin, S. S.; Zombeck, J. A.; Wu, C.; Yau, P. M.; Gao, P.; van Nispen, A. J.; Patrie, S. M.; Thomas, P. M.; Sweedler, J. V.; Rhodes, J. S.; Kelleher, N. L. Top-Down Proteomics Enables Comparative Analysis of Brain Proteoforms Between Mouse Strains. *Analytical chemistry* **2018**, *90*, 3802−3810.
(46) Ghandour, M. S.; Parkkila, A.-K.; Parkkila, S.; Waheed, A.; Sly, W. S. Mitochondrial Carbonic Anhydrase in the Nervous System. *Journal of Neurochemistry* **2000**, *75*, 2212−2220.
(47) Liu, G.; Zhang, C.; Yin, J.; Li, X.; Cheng, F.; Li, Y.; Yang, H.; Uéda, K.; Chan, P.; Yu, S. α-Synuclein is differentially expressed in mitochondria from different rat brain regions and dose-dependently down-regulates complex I activity. *Neurosci. Lett.* **2009**, *454*, 187−192.
(48) Delcourt, V.; Franck, J.; Quanico, J.; Gimeno, J.-P.; Wisztorski, M.; Raffo-Romero, A.; Kobeissy, F.; Roucou, X.; Salzet, M.; Fournier, I. Spatially-Resolved Top-down Proteomics Bridged to MALDI MS Imaging Reveals the Molecular Physiome of Brain Regions. *Mol. Cell Proteomics* **2018**, *17*, 357−372.
(49) Hashimoto, M.; Rockenstein, E.; Mante, M.; Mallory, M.; Masliah, E. β-Synuclein Inhibits α-Synuclein Aggregation: A Possible Role as an Anti-Parkinsonian Factor. *Neuron* **2001**, *32*, 213−223.
(50) Park, J.-Y.; Lansbury, P. T. β-Synuclein Inhibits Formation of α-Synuclein Protofibrils: A Possible Therapeutic Strategy against Parkinson's Disease. *Biochemistry* **2003**, *42*, 3696−3700.
(51) Alkam, D.; Feldman, E. Z.; Singh, A.; Kiaei, M. Profilin1 biology and its mutation, actin(g) in disease. *Cell. Mol. Life Sci.* **2017**, *74*, 967−981.
(52) Krishnan, K.; Moens, P. D. J. Structure and functions of profilins. *Biophys Rev.* **2009**, *1*, 71−81.
(53) Rajkumar, K.; Nichita, A.; Anoor, P. K.; Raju, S.; Singh, S. S.; Burgula, S. Understanding perspectives of signalling mechanisms regulating PEBP1 function. *Cell Biochemistry and Function* **2016**, *34*, 394−403.
(54) Wang, Z.; Bu, J.; Yao, X.; Liu, C.; Shen, H.; Li, X.; Li, H.; Chen, G. Phosphorylation at S153 as a Functional Switch of Phosphatidylethanolamine Binding Protein 1 in Cerebral Ischemia-Reperfusion Injury in Rats. *Front. Mol. Neurosci.* **2017**, *10*, 358.
(55) Shao, S.; Fan, Y.; Zhong, C.; Zhu, X.; Zhu, J. Coactosin-Like Protein (COTL1) Promotes Glioblastoma (GBM) Growth in vitro and in vivo. *Cancer Manag Res.* **2020**, *12*, 10909−10917.
(56) Irvine, G. B.; El-Agnaf, O. M.; Shankar, G. M.; Walsh, D. M. Protein aggregation in the brain: the molecular basis for Alzheimer's and Parkinson's diseases. *Mol. Med.* **2008**, *14*, 451−464.
(57) Tamás, M. J.; Sharma, S. K.; Ibstedt, S.; Jacobson, T.; Christen, P. Heavy metals and metalloids as a cause for protein misfolding and aggregation. *Biomolecules* **2014**, *4*, 252−267.

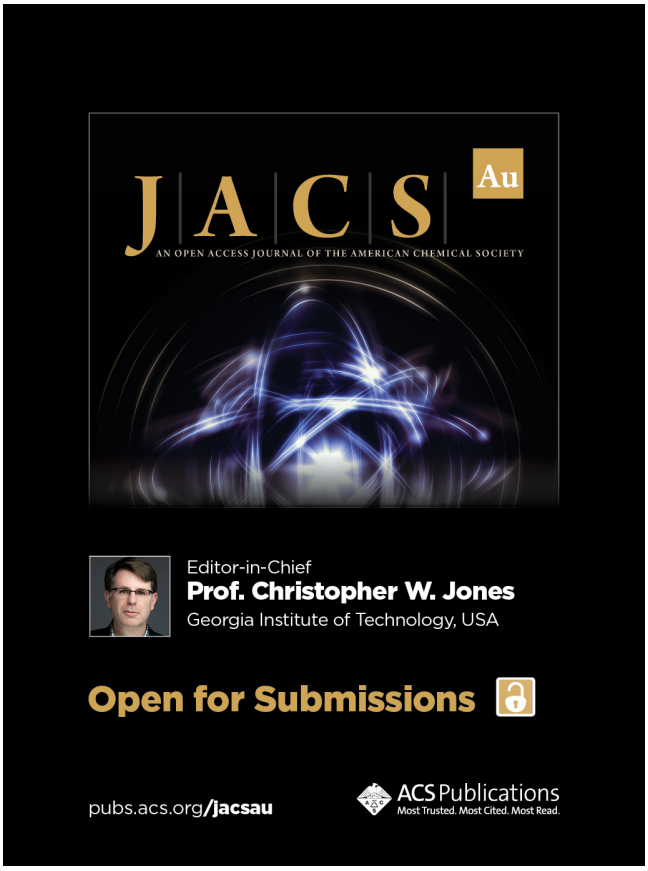

https://doi.org/10.1021/jacs.1c10032
J. Am. Chem. Soc. 2022, 144, 2120−2128